

**DEVELOPMENT OF TETRAGONAL ZIRCONIA THIN FILM FOR  
SEMICONDUCTOR APPLICATION**

**CHAN POOI QUAN**

**August 2011**

**DEVELOPMENT OF TETRAGONAL ZIRCONIA THIN FILM FOR  
SEMICONDUCTOR APPLICATION**

**by**

**CHAN POOI QUAN**

**Thesis submitted in fulfillment of the requirements  
for the degree of  
Master of Science**

**August 2011**

## ACKNOWLEDGEMENT

First of all, I would like express my deepest appreciation to my principal supervisor, Prof. Ahmad Fauzi bin Mohd. Noor, who had gives his guidance and constant support along these years. His wide knowledge and logical thinking have been inspiring and led me to complete my research. I would like to convey my gratitude to my co-supervisor, Prof. Madya Dr. Zainovia bt. Lockman and Dr. Yeoh Fei Yee for their important advices and technical supports in completing this work.

I am grateful and appreciative to all the lecturers, administration and technical staffs in School of Materials and Mineral Resources Engineering, USM for their precious help and technical support. I am particularly indebted to Mr. Suhaimi and Mrs. Fong for their enormous support and kind assistance.

I would like to thank USM-RU-PRGS Grant (1001/PBAHAN/8032023), E-Science Fund Grant (MOSTI) (account number: 6013342) and USM fellowship for the funding and financial support throughout my research work.

Lastly, I also like to thank all my group members particularly Uday, Umar, Nilar, Tony, Nazida, Sunarso, Sengphet, Yanny, Mizam, Kee, Chong and Eunisse for the friendship, cooperation and the enjoyable working environment. Special gratitude to my family and beloved friends (PTA) for their love, unfailing encouragement and moral supports during my Master study. "Friends are the most important ingredient in this recipe of life".

## TABLE OF CONTENT

	<b>Page</b>
<b>ACKNOWLEDGEMENT</b>	<b>ii</b>
<b>TABLE OF CONTENTS</b>	<b>iii</b>
<b>LIST OF TABLES</b>	<b>vii</b>
<b>LIST OF FIGURES</b>	<b>x</b>
<b>LIST OF ABBREVIATIONS</b>	<b>xvi</b>
<b>LIST OF PUBLICATIONS</b>	<b>xvii</b>
<b>ABSTRAK</b>	<b>xviii</b>
<b>ABSTRACT</b>	<b>xix</b>
<b>CHAPTER 1: INTRODUCTION</b>	
1.1 Background	1
1.2 Problem Statement	3
1.3 Objective	3
1.4 Project Overview	4
<b>CHAPTER 2: LITERATURE REVIEW</b>	
2.1 Introduction	5
2.2 Zirconia (ZrO <sub>2</sub> )	5
2.2.1 Polymorph	6
2.3 Phase Transition	7
2.3.1 Phase Transformation of Tetragonal $\rightleftharpoons$ Cubic	8
2.3.2 Phase Transformation of Monoclinic $\rightleftharpoons$ Tetragonal	8
2.4 Stabilizer ZrO <sub>2</sub>	9

2.4.1	Yttria Stabilized Zirconia (YSZ)	10
2.4.2	Niobia-Yttria Stabilized Zirconia (Nb-YSZ)	13
2.5	Comparison between Thin Film and Bulk Ceramics	14
2.6	Thin Film Deposition Technique	16
2.7	Chemical Solution Deposition (CSD)	18
2.7.1	Coating Solute	19
2.7.1(a)	Metal Organic Decomposition (MOD)	20
2.7.2(b)	Sol Gel Methods	20
2.7.2	Coating Solvents	22
2.7.3	Substrate	23
2.7.4	Coating Techniques	24
2.7.4(a)	Dip Coating	25
2.7.5	Heat Treatment	28
2.8	Electronic Structure	29
2.9	Application	31

### **CHAPTER 3: METHODOLOGY**

3.1	Introduction	35
3.2	Raw Material	37
3.3	Preparation of Precursor Solution	38
3.3.1	Synthesis of YSZ Sol	38
3.3.2	Synthesis of Nb-doped YSZ Sol	39
3.4	Cleaning Produce	41
3.4.1	Glass Cleaning	41
3.4.2	Wafer Cleaning	41

3.5	Dip Coating Process	42
3.6	Annealing Stage	43
3.7	Experiment Design	43
3.8	Characterizations	46
3.8.1	Thermogravimetric Analysis (TGA)	46
3.8.2	X-Ray Diffraction (XRD)	46
3.8.3	Optical Microscope (OM)	48
3.8.4	Field Emission Scanning Electron Microscope (FESEM)	48
3.8.5	Energy-Dispersive X-Ray Spectrometer (EDS)	48
3.8.6	Atomic Force Microscope (AFM)	49
3.8.7	Ultraviolet-visible Spectroscopy (UV-vis)	49

## **CHAPTER 4: RESULTS AND DISCUSSION**

4.1	Introduction	51
4.2	Thermogravimetric Analysis of YSZ Powder	51
4.3	YSZ Thin Film Formation on Silica Glass	53
4.3.1	Effect of Number of Coatings	53
4.3.2	Effect of Precursor Solution Concentration	62
4.3.3	Effect of Annealing Temperature	70
4.3.4	Effect of Heating Rate	79
4.4	YSZ Thin Film Formation on Si <100> Wafer	85
4.4.1	Effect of Number of Coatings	85
4.4.2	Effect of Precursor Solution Concentration	94
4.4.3	Effect of Annealing Temperature	101

4.4.4	Effect of Heating Rate	111
4.5	Comparison between YSZ Film Coated on Silica Glass and Si Wafer	117
4.6	Effect of Addition of Niobium into the Starting Sol	120
4.6.1	Deposition on Silica Glass	120
4.6.2	Deposition on Si Wafer	126
 <b>CHAPTER 5: CONCLUSIONS AND RECOMMENDATION</b>		
5.1	Conclusion	131
5.2	Recommendation for Future Development	132
 <b>REFERENCES</b>		
 <b>APPENDICES</b>		
		146

## LIST OF TABLES

		<b>Page</b>
Table 2.1	Deposition techniques and their respective definition.	17
Table 2.2	Summary of different deposition techniques used for YSZ films in recent years and the related authors.	18
Table 2.3	Direct band gap energy (eV) of ZrO <sub>2</sub> from different research works.	31
Table 2.4	Application of ZrO <sub>2</sub> -based bulk materials.	31
Table 3.1	Detail for raw materials.	37
Table 3.2	Mass for raw material required for different concentration of YSZ sol.	39
Table 3.3	Mass for raw material required for different concentration of Nb-YSZ sol.	40
Table 3.4	Characteristic of optimum YSZ and Nb-YSZ film.	44
Table 3.5	Summary of the YSZ and Nb-YSZ film formation on silica glass and Si Wafer at different parameter.	45
Table 3.6	ICDD numbers used for characterize the sample.	47
Table 4.1	Optical microscope images for the sample after annealing as a function of the number of coatings.	54
Table 4.2	The average thickness of the film with different number of coatings.	58
Table 4.3	Optical microscope image for the sample after annealing as a function of precursor solution concentration.	62
Table 4.4	The average thickness of the film prepared with different concentration of precursor solutions.	66
Table 4.5	Schematic diagram of the film formation as a function of the concentration of precursor solution.	68
Table 4.6	Optical microscope image for the sample annealed at different temperature.	70
Table 4.7	Crystallite size for the sample annealed at 450 °C to 600°C.	73



Table 4.8	The average thickness of film annealed with different temperatures.	75
Table 4.9	Optical microscope images for the sample annealed at 550 °C with different heating rates.	79
Table 4.10	The average thickness of film with different heating rates.	83
Table 4.11	Optical microscope images for the sample after annealing as a function of the number of coatings.	86
Table 4.12	The average thickness of film with different number of coatings.	90
Table 4.13	Optical microscope image for the sample prepared with different concentration of precursor solution.	95
Table 4.14	The average thickness of film with different concentration of precursor solutions.	99
Table 4.15	Optical microscope image for the sample annealed at different temperatures.	102
Table 4.16	Crystallite size for the film annealed at different temperatures.	105
Table 4.17	The average thickness of film with different annealing temperatures.	107
Table 4.18	Comparison between the grain size and thickness of the film.	109
Table 4.19	Optical microscope images for the coatings annealed at 600 °C with different heating rate.	111
Table 4.20	The average thickness of film annealed with different heating rates.	115
Table 4.21	The optimum parameters for the silica glass and Si wafer substrates.	118
Table 4.22	Film properties for the film coated on silica glass and Si wafer.	119
Table 4.23	Optical microscope images for the film on silica glass prepared with Nb-YSZ sol.	121
Table 4.24	The average thickness of film prepared with Nb-YSZ and YSZ sol.	124

Table 4.25	Optical microscope images for the film on Si wafer prepared with Nb-YSZ sol.	126
Table 4.26	The average thickness of film prepared with Nb-YSZ and YSZ sol.	129

## LIST OF FIGURES

		<b>Page</b>
Figure 2.1	Polymorph $ZrO_2$ : (a) cubic, (b) tetragonal, and (c) monoclinic.	6
Figure 2.2	A pseudo-fluorite cell of tetragonal zirconia. The arrows show the displacement of the oxygen ions along the c-axis.	8
Figure 2.3	Phase change from a tetragonal to monoclinic form.	9
Figure 2.4	Phase diagram for $ZrO_2$ - $Y_2O_3$ .	11
Figure 2.5	Effect of Y doping on $ZrO_2$ fluorite structure.	12
Figure 2.6	Preparation stages for thin film and bulk ceramics by using sol-gel method.	15
Figure 2.7	Flow Chart of a typical chemical solution deposition (CSD) process.	19
Figure 2.8	The common used coating techniques.	24
Figure 2.9	Fundamental stages of sol-gel dip coating (the arrows indicate the flow of solution).	26
Figure 2.10	Band Structure for (a) and (b) conductor, (c) semiconductor and (d) insulator.	30
Figure 3.1	Flow Chart of the experimental work.	36
Figure 3.2	Flow chart for the preparation of YSZ sol.	39
Figure 3.3	Flow chart for the preparation of Nb-doped YSZ sol.	40
Figure 3.4	Deposition procedure for multiple coatings	42
Figure 3.5	Heating schedule for coated substrate	43
Figure 3.6	Parameters for the experiment.	44
Figure 4.1	TGA curve for the mixture $ZrOCl_2 \cdot 8H_2O$ and $YNO_3 \cdot 6H_2O$ precursor salt.	52
Figure 4.2	XRD patterns of the coatings formed on silica glass after being annealed at 500 °C for 30 min. The samples were coated with (a) 1, (b) 3 and (c) 5 times of coatings. The enlarged XRD plotted from 50° to 52°.	56

Figure 4.3	FESEM images of the coatings formed on silica glass. The numbers of coatings were (a) 1, (b) 3 and (c) 5 times. The magnifications of the FESEM images were 100 kX.	57
Figure 4.4	EDX compositional analysis for sample prepared with 3 coatings. (a) Surface morphology and (b) table for element in at%.	58
Figure 4.5	FESEM images showing the cross section view of film with (a) 1, (b) 3 and (c) 5 coatings.	58
Figure 4.6	AFM images of films prepared with (a) 1, (b) 3 and (c) 5 coatings.	59
Figure 4.7	Schematic diagram of the film formation with different number of coatings.	60
Figure 4.8	Optical band gap value for the film with different number of coating: (a) 1, (b) 3 and (c) 5 times.	61
Figure 4.9	XRD patterns of the coatings formed on silica glass as a function of the concentration of solution: (a) 0.2 mol, (b) 0.4 mol and (c) 0.6 mol. The enlarged XRD plotted from 50° to 52°.	64
Figure 4.10	FESEM image of the coatings prepared with different concentration of precursor solution: (a) 0.2 mol, (b) 0.4 mol and (c) 0.6 mol. The magnifications of the FESEM images were 100 kX.	65
Figure 4.11	Cross section view of the film deposited with (a) 0.2 mol, (b) 0.4 mol and (c) 0.6 mol precursor solution.	66
Figure 4.12	AFM images of films prepared with concentration (a) 0.2 mol, (b) 0.4 mol and (c) 0.6 mol.	67
Figure 4.13	Optical band gap value for the film prepared with different concentration of precursor solution: (a) 0.2 mol and (b) 0.4 mol.	69
Figure 4.14	XRD patterns for the coating annealed at different temperature: (a) 450 °C, (b) 500 °C, (c) 550 °C and (d) 600 °C. The enlarged XRD plotted from 50° to 52°.	72
Figure 4.15	FESEM images for coating after annealed at (a) 450°C, (b) 500°C, (c) 550°C and (d) 600°C for 30 minutes. The magnifications of the FESEM images were 100 kX.	73

Figure 4.16	Cross section view for the film annealed at (a) 450°C, (b) 500°C and (c) 550°C.	75
Figure 4.17	AFM images for films annealed at (a) 450°C, (b) 500°C and (c) 550°C.	76
Figure 4.18	Schematic diagram of the formation of the film when annealed at different temperatures.	77
Figure 4.19	Optical band gap value for the film annealed at different temperatures: (a) 450 °C, (b) 500 °C and (c) 550 °C.	78
Figure 4.20	XRD patterns of the coatings annealed at 550 °C with different heating rates: (a) 1.5 °C/min, (b) 5 °C/min and (c) 10 °C/min. The enlarged XRD plotted from 50° to 52°.	81
Figure 4.21	FESEM images of the films annealed with different heating rate: (a) 1.5 °C/min, (b) 5 °C/min, and (c) 10 °C/min. The magnification of the images was 100 kX.	82
Figure 4.22	Cross section view for the film annealed at 550 °C for 30 min with heating rate (a) 1.5 °C/min and (b) 5 °C/min.	83
Figure 4.23	AFM images of the films annealed with heating rate: (a) 1.5 °C/min, (b) 5 °C/min, and (c) 10 °C/min.	84
Figure 4.24	Optical band gap value for the film annealed at 550 °C for 30 minutes with different heating rates: (a) 1.5 °C/min and (b) 5 °C/min.	85
Figure 4.25	XRD patterns of the coatings formed on Si wafer. The samples were coated with (a) 1, (b) 3 and (c) 5 times. The enlarged XRD plotted from 50° to 52°.	88
Figure 4.26	FESEM image of the films on silica glass with different number of coatings: (a) 1, (b) 3 and (c) 5 times. The magnification of the images was 100 kX.	89
Figure 4.27	FESEM images showing the cross section view of film with (a) 1, (b) 3 and (c) 5 coatings.	90
Figure 4.28	EDX compositional analysis for the film with 3 coatings: (a) cross section morphology and (b) table for element in at% for point A and B.	91
Figure 4.29	AFM images of the coating prepared with (a) 1, (b) 3 and (c) 5 coatings.	91

Figure 4.30	Optical band gap value for the film prepared with (a) 1, (b) 3 and (c) 5 coatings.	92
Figure 4.31	Schematic diagram for the film coated on (a) silica glass and (b) Si wafer substrates.	94
Figure 4.32	XRD patterns for the films prepared with concentration (a) 0.2 mol, (b) 0.4 mol and (c) 0.6 mol precursor solution. The enlarged XRD plotted from 50° to 52°.	97
Figure 4.33	FESEM image of the coating on Si wafer prepared with concentration: (a) 0.2 mol, (b) 0.4 mol and (c) 0.6 mol precursor solution. The magnification of the images was 100 kX.	98
Figure 4.34	Cross section view of the film prepared with (a) 0.2 mol, (b) 0.4 mol and (c) 0.6 mol precursor solution.	99
Figure 4.35	AFM images of the films prepared with concentration (a) 0.2 mol, (b) 0.4 mol, and (c) 0.6 mol precursor solution.	100
Figure 4.36	Optical band gap value for the film prepared with concentration (a) 0.2 mol and (b) 0.4 mol precursor solution.	101
Figure 4.37	XRD patterns for the coatings annealed at temperatures (a) 500 °C, (b) 550 °C, (c) 600 °C and (d) 650 °C. The enlarged XRD plotted from 50° to 52°.	104
Figure 4.38	FESEM images for the films annealed at temperatures (a) 500°C, (b) 550°C, (c) 600°C and (d) 650°C. The magnification of the images was 100 kX.	105
Figure 4.39	Cross sections of the film annealed at temperatures (a) 500°C, (b) 550°C, (c) 600°C and (d) 650°C.	106
Figure 4.40	The AFM image for the films annealed at temperatures 500 °C, (b) 550 °C, (c) 600 °C and (d) 650 °C.	107
Figure 4.41	Schematic representative of grain clustering phenomenon in doped-ZrO <sub>2</sub> film. The grain size, D, is greater than the thickness of the layer, t.	108
Figure 4.42	Optical band gap for the film on Si wafer annealed at temperature (a) 500 °C, (b) 550 °C, (c) 600 °C and (d) 650 °C.	110

Figure 4.43	XRD patterns for the films annealed at 600 °C with heating rate (a) 1.5 °C/min, (b) 5 °C/min and (c) 10 °C/min. The enlarged XRD plotted from 50° to 52°.	113
Figure 4.44	FESEM image for the films annealed with heating rates: (a) 1.5 °C/min, (b) 5 °C/min, and (c) 10 °C/min. The magnification of the images was 100 kX.	114
Figure 4.45	Cross sections view for the film annealed with heating rates: (a) 1.5 °C/min, (b) 5 °C/min, and (c) 10 °C/min.	115
Figure 4.46	AFM image of the films annealed at 600 °C with heating rate (a) 1.5°C/min, (b) 5°C/min and (c) 10°C/min.	116
Figure 4.47	Optical band gap for the film annealed at 600 °C with heating rate (a) 1.5 °C/min, (b) 5 °C/min and (c) 10 °C/min.	117
Figure 4.48	XRD patterns for the film prepared by solution (a) Nb-YSZ and (b) YSZ. The enlarged XRD plotted from 50° to 52°.	122
Figure 4.49	FESEM image for the film made by solution with addition of Nb at magnification (a) 20 kX and (b) 100 kX.	123
Figure 4.50	EDX analysis for the film prepared with Nb-YSZ sol. (a) FESEM image and (b) Table for element in at% for point A and B	123
Figure 4.51	Cross section view of the film on silica glass prepared with solution (a) Nb-YSZ and (b) YSZ.	124
Figure 4.52	Optical band gap value for the sample prepared with solution (a) Nb-YSZ and (b) YSZ.	125
Figure 4.53	XRD patterns for the film prepared by solution (a) Nb-YSZ and (b) YSZ. The enlarged XRD plotted from 50° to 52°.	127
Figure 4.54	FESEM image for the film made by solution with addition of Nb at magnification (a) 20 kX and (b) 100 kX.	128
Figure 4.55	EDX analysis for the film prepared with Nb-YSZ sol. (a) SEM image and (b) Table for element in at% for point A and B.	128
Figure 4.56	Cross section view of the film on Si wafer prepared with solution (a) Nb-YSZ and (b) YSZ.	129

Figure 4.57 Optical band gap value for the sample prepared with solution (a) Nb-YSZ and (b) YSZ. 130



## LIST OF ABBREVIATIONS

AFM	Atomic Force Microscopy
CSD	Chemical Solution Deposition
CVD	Chemical Vapour Deposition
EDS	Energy-dispersive Spectrometer
EPD	Electrophoretic Deposition
FSZ	Fully Stabilized Zirconia
FESEM	Field Emission Scanning Electron Microscopy
ICDD	International Centre for Diffraction Data
MOD	Metal Organic Decomposition
Nb <sub>2</sub> O <sub>5</sub>	Niobium oxide
Nb-YSZ	Niobium doped Ytria Stabilized Zirconia
OM	Optical Microscopy
PLD	Pulsed Laser Depositions
PSZ	Partially Stabilized Zirconia
TGA	Thermogravimetric Analysis
TZP	Tetragonal Zirconia Polycrystals
UV-vis	Ultraviolet-visible Spectroscopy
XRD	X-ray Diffraction
Y <sub>2</sub> O <sub>3</sub>	Yttrium Oxide
YSZ	Ytria Stabilized Zirconia
ZrO <sub>2</sub>	Zirconia

## LIST OF PUBLICATIONS

1. Chan Pooi Quan, Ahmad Fauzi M.N., Zainovia Lockman, Yeoh Fei Yee  
Preparation of yttria-stabilized zirconia thin film on Si wafer by using dip coating. 4<sup>th</sup> Colloquium on Postgraduate Research: National Postgraduate Colloquium on Materials, Minerals and Polymers 2010. 27<sup>th</sup> and 28<sup>th</sup> January 2010. Vistana Hotel, Penang.
2. Chan Pooi Quan, Ahmad Fauzi M.N., Zainovia Lockman, Yeoh Fei Yee  
(2009) Preparation of doped zirconia thin film by using dip coating. 11<sup>th</sup> International Conference on Electronic Materials and Packaging. 1<sup>st</sup> - 3<sup>rd</sup> December 2009. Penang, Malaysia.

# PEMBANGUNAN FILEM NIPIS ZIRKONIA TETRAGONAL UNTUK KEGUNAAN SEPARA PENGALIR

## ABSTRAK

Dalam penyelidikan ini, filem YSZ dan Nb-YSZ dihasil melalui kaedah pemendapan larutan kimia dengan menggunakan kaedah salut celup. Filem akan dibentuk atas dua jenis substrat (kaca silika dan wafer Si). Pelbagai parameter telah dikaji dalam penyelidikan ini termasuklah bilangan celupan, kepekatan larutan prapenanda, suhu penyepuhlindungan dan kadar pemanasan untuk memperolehi keadaan optimum bagi filem dengan kualiti salutan yang terbaik. Larutan prapenanda disediakan atas nisbah molar bagi  $ZrOCl_2 \cdot 8H_2O$  dan  $YNO_3 \cdot 6H_2O$  ialah 95:5 dan mencampur dengan etanol mutlak sebagai pelarut. Kesan penambahan  $Nb(OC_2H_5)_5$  ke dalam larutan prapenanda YSZ dengan nisbah molar 90:5:5 juga dikaji. Filem yang licin dan tanpa retakan boleh dihasilkan apabila substrat mencelup 3 kali ke dalam 0.4 mol larutan prapenanda. Kehabluran yang baik,  $ZrO_2$  yang berfasa tetragonal boleh dibentuk apabila filem penyepuhlindungan di suhu 550 °C atas substrat kaca dan 600 °C atas wafer Si dalam 30 minit dengan kadar pemanasan 1.5°C/min. Kekasaran permukaan, RMS bagi filem adalah lebih kurang 3 nm. Di bawah keadaan optimum, ketebalan bagi filem adalah dalam julat 150 nm hingga 200 nm. Analisis UV-vis dijalankan untuk memperolehi sela jalur optik bagi filem. Sela jalur tenaga bagi filem dibentuk atas kaca silika adalah 2.60 eV dan wafer Si adalah 2.46 eV. Namun begitu, bagi penambahan Nb, keputusan menunjukkan selar jalur tenaga bagi filem adalah hampir sama apabila berbanding dengan filem YSZ.

# DEVELOPMENT OF TETRAGONAL ZIRCONIA THIN FILM FOR SEMICONDUCTOR APPLICATION

## ABSTRACT

In this work, the YSZ and Nb-YSZ film were produced by using chemical solution deposition (CSD) technique via dip coating. The films were deposited on two different substrates (silica glass and Si wafer). Various parameters were conducted in this study including numbers of coatings, concentration of precursor solution, annealing temperature and heating rate to obtain the optimum condition for coating of the film. The precursor solution was prepared with the molar ratio of  $\text{ZrOCl}_2 \cdot 8\text{H}_2\text{O}$  to  $\text{YNO}_3 \cdot 6\text{H}_2\text{O}$  at 95:5 and mixed with absolute ethanol as a solvent. The effect of addition of  $\text{Nb}(\text{OC}_2\text{H}_5)_5$  into the YSZ precursor solution with molar ratio 90:5:5 was also studied. Smooth and crack-free film was produced when the substrate was dipped 3 times into 0.4 mol precursor solution. Tetragonal phase  $\text{ZrO}_2$  was formed when the film was annealed at temperature 550 °C on glass substrate and 600 °C on Si wafer in 30 minutes with heating rate 1.5 °C/min. The films had adhered well on the substrate. The surface roughness, RMS of the film was around 3 nm. Under the optimized condition, the thickness of the films was in the range of 150 nm to 200 nm. UV-vis analysis was carried out to obtain the optical band gap of the films. The band gap energy for the film coated on silica glass was 2.60 eV and Si wafer was 2.45 eV. However, with addition of Nb, the result showed that the band gap energy of the film was similar when compared to YSZ film.

# CHAPTER 1

## INTRODUCTION

### 1.1 Background

Zirconia ( $ZrO_2$ ) was one of the earliest ceramics in which conduction by oxygen ions was observed. Subsequently, this characteristic has been exploited in fuel cell and sensor technologies [Muñoz et al., 2006].  $ZrO_2$ -based ceramics has attracted attention for the use as engineering ceramic for mechanical and electronic purposes [Patil et al., 2008].

Traditionally,  $ZrO_2$  ceramic was prepared in bulk form. However, recently it has been developed as thin film for wider application, such as solid oxide fuel cells (SOFC) [Wang et al., 2007] and thermal barrier coatings (TBCs) [Sun et al., 2010]. When it is applied as a thin film, it have many advantages including compact dimensions with smaller power consumption, reduced ohmic losses and lower operating temperature. Typically,  $ZrO_2$  based ceramic in thin film have low thermal conductivity ( $2.7 \text{ W.m}^{-1}.\text{K}^{-1}$ ), a relative high dielectric constant (26 MHz), high electrical resistivity ( $>10^{13} \text{ Wcm}$ ), extreme chemical inertness and high ionic conductivity [Kuo et al., 2002; Torres-Huerta et al., 2009; FerroCeramic, 2005].

There are several semiconductor fabrication techniques that are used to fabricate  $ZrO_2$  film. These include sputtering [Ben Amor et al., 1998; Kuo and Chien, 2003], chemical vapour deposition [Goto, 2004] and spray pyrolysis [López Ibáñez et al., 2006]. Chemical Solution deposition (CSD) is also frequently employed and

modified for the preparation of thin film because it is simple, feasible, low deposition temperatures and do not require costly equipment [Chang and Doong, 2005]. The use of CSD in this project is seen as interesting and efficient way to produce a good quality film.

Generally, ceramics has wide range of electrical properties including insulating, semiconducting, superconducting, piezoelectric and magnetic. Zirconia is typically classified as an electrical insulator because of its wide band gap (5.1-7.8 eV) [Jeong et al., 2005]. However, high temperature stability and high toughness makes zirconia possible to be used as wide band gap electronic material by doping suitable stabilizing oxides. The electronic material requires wide band gap (3 – 4 eV) for high voltage and high temperature operation with good transport properties [Kumari et al., 2009].

With this background, zirconia was prepared as thin film in this study by doping with yttrium ( $Y^{3+}$ ) and niobium ( $Nb^{5+}$ ). The addition of stabilizing oxides,  $Y_2O_3$  into the  $ZrO_2$  allows the retention of the tetragonal phase at room temperature and leading to high toughness [Denry and Kelly, 2008]. Ytria-stabilized zirconia (YSZ) also exhibits a number of properties (e.g. good corrosion resistance and high refractive index) which results in great interest in theoretical studies and in practical application [Xiao et al., 2009]. Tetragonal phase was preferred in this project because the pure t- $ZrO_2$  exhibits the band gap in around 3 eV [Muñoz et al., 2006]. The high mechanical and high toughness properties ( $8-13 \text{ MPa m}^{-1/2}$ ) also make it suitable to fabricate  $ZrO_2$  in thin film [Galdikas et al., 2008].  $Nb^{5+}$  was used as electronic dopant to lower the band gap of zirconia and to provide the free electron. The Nb-Y-Zr

could be use in high power and high temperature devices like sensors and switches in automobile.

## **1.2 Problem Statement**

The previous work showed that when  $\text{Nb}_2\text{O}_3$  was added into YSZ powder, it reduced the band gap from 6.09 eV to 4.00 eV [Niki, 2007]. Addition of  $\text{Nb}_2\text{O}_5$  was successfully substituted into the YSZ lattice. However, the tetragonal phase for Nb-YSZ powder had transformed to a mixed phase of tetragonal and monoclinic when prepared in pellet form and sintered at high temperature (1250 °C - 1550 °C) [Niki, 2007]. To overcome this problem, Nb-YSZ was suggested to prepare in thin film to reduce the annealing temperature while retaining the tetragonal phase, as well as the required physical and electrical properties.

## **1.3 Objective**

The main objective of this work was to produce tetragonal Nb-YSZ film with low band gap ( $< 4$  eV) for semiconducting applications. Generally this study involved:

1. The effect of number of coatings, precursor solution concentration, annealing temperature and heating rate on the formation of Yittra-stabilized-zirconia film.
2. Investigate the effect of substrate (silica glass and Si wafer) for doped-zirconia film.
3. Investigate the effect of addition  $\text{Nb}^{5+}$  to Yittria-stabilized-Zirconia (i.e. if the tetragonal phase retained) and the band gap value.

#### **1.4 Project Overview**

A sol-gel dip-coating method was chosen to produce the doped-ZrO<sub>2</sub> thin film. The doped-ZrO<sub>2</sub> thin film was coated on two different substrates: silica glass substrate and N-type Si <100> wafer to study the influence of substrate to the film properties. The project was divided into two phases: the first phase was to investigate the optimum condition (coating cycles, sol concentration, heat treatment temperature, heating rate) for YSZ film. The second phase uses the optimum condition observed from the first phase to produce Nb-YSZ thin film. Various parameters were studied in this project to investigate their influence on the surface morphology and crystallite phase for doped-ZrO<sub>2</sub> film.

Characterization method used in this project include X-ray Diffraction (XRD), Field Emission Scanning Electron Microscopy (FESEM), Energy-dispersive X-ray Spectrometer (EDS), Atomic Force Microscopy (AFM), Optical Microscopy (OM), Ultraviolet-visible Spectroscopy (UV-Vis) and Thermogravimetric analysis (TGA).



## CHAPTER 2

### LITERATURE REVIEW

#### 2.1 Introduction

In recent years, zirconia ( $ZrO_2$ ) in thin film has found increasing attention due to the rise in new field of application.  $ZrO_2$  film is an extremely versatile ceramic that has been use in oxygen pumps and sensors, fuel cells, thermal barrier coating, and other high-temperature applications, which take advantages of the electrical, thermal, and mechanical properties of  $ZrO_2$  [Shackelford and Doremus, 2008].

In this chapter, a brief review of the  $ZrO_2$  structure and its properties is presented. The addition of stabilizing oxides to retain tetragonal phase is reviewed. As  $Y^{3+}$  and  $Nb^{5+}$  dopants are mostly concerned in this work, the mechanism will be discussed.  $ZrO_2$ -based thin film can be prepared by various deposition techniques. The chemical solution deposition (CSD) technique is preferred due to its flexible process parameter and the deposition process will be presented in depth. The potentials applications of  $ZrO_2$ -based thin film will also be discussed.

#### 2.2 Zirconia ( $ZrO_2$ )

Zirconium contains  $Zr^{4+}$  ion and forms a single oxide, zirconia ( $ZrO_2$ ) with 2 oxygen ions,  $O^{2-}$ . Pure or mixed with other oxides,  $ZrO_2$  is one of the most studied ceramic materials due to its high strength (1000 - 1800 MPa), thermal stability (melting point 2680 °C), high wear resistance, electrical resistivity ( $>10^{13}$  Wcm), high dielectric constant (26 MHz) and being chemically inert. It could enhance the

mechanical properties of other ceramics when uniformly dispersed in their matrices when forming a composite [Wang et al., 2009; Patil et al., 2008].

The crystalline polymorph phase of zirconia, i.e. monoclinic, tetragonal, cubic, or a mixture of these phases can be obtained depending on the preparation method and thermal treatment. To use the  $ZrO_2$  in full potential, the properties of the oxide have to be modified by addition of stabilizing oxide [Rosa et al., 2008]. Hence, bulk material or thin film  $ZrO_2$  can be produced for different purposes.

### 2.2.1 Polymorph

$ZrO_2$  can exist in three structural forms: monoclinic (m) phase stable at temperatures below 1170 °C, tetragonal (t) structure formed at temperatures between 1170 °C and 2370 °C while cubic (c) phase remain stable from temperatures 2370 °C until the melting point of  $ZrO_2$  [Yang et al., 2008; Zavodinsky and Chibisov, 2006]. The crystal structures for three polymorph are shown in Figure 2.1.

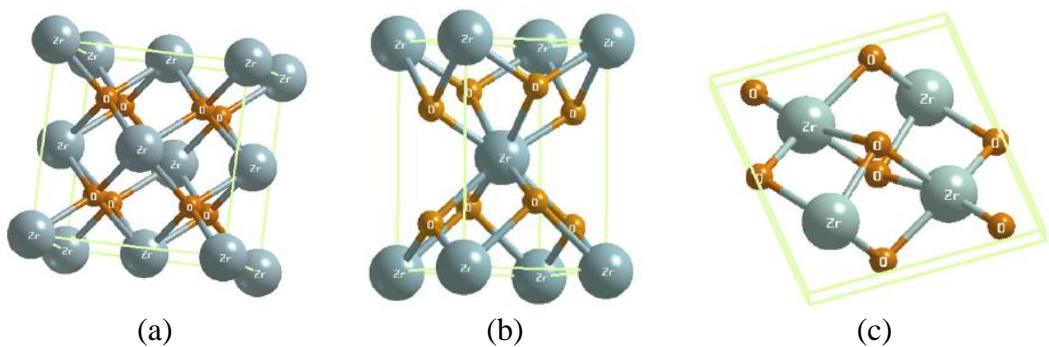
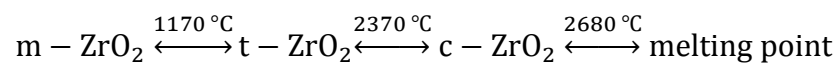


Figure 2.1: Polymorph  $ZrO_2$ : (a) cubic, (b) tetragonal, and (c) monoclinic [Terki et al., 2006].

c-ZrO<sub>2</sub> has a fluorite structure, where the Zr atoms form a fcc lattice and the oxygen atoms occupy the tetrahedral interstitial sites associated with the fcc lattice. The cubic structure exhibits single lattice constant,  $a$  [Muñoz et al., 2006].

t-ZrO<sub>2</sub> derived its structure from cubic fluorite structure with the oxygen atoms placed along one of the cubic axes and cause the tetragonal distortion along that axis. The tetragonal structure was specified by the two lattice parameters,  $a$  and  $c$ . The Zr ions are again eight-fold coordinated to O, with four oxygen neighbours arranged in a flattened tetrahedron at a short Zr–O distance of 2.065 Å, and the rest in an elongated tetrahedron rotated 90° at a distance of 2.455 Å from Zr [Muñoz et al., 2006]. On the other hand, the monoclinic form has a complex geometric structure with a 12-atom primitive cell. It consists of layers of triangular coordination polyhedra for three  $O_I$ -Zr bonds and four distorted tetrahedral  $O_{II}$ -Zr bonds for a total seven oxygen ions surrounding the zirconium. Lattice parameters,  $a$ ,  $b$ ,  $c$ ,  $\beta$  and internal parameters,  $x$ ,  $y$ ,  $z$  for Zr,  $O_I$ ,  $O_{II}$  are needed to specify the structure.

### 2.3 Phase Transition

The temperature at which both forms of ZrO<sub>2</sub> are in equilibrium is called the transition temperature. Although only small ionic movements are involved at this temperature, there may be marked changes in various properties. This could alter the crystal dimensions and result in development of internal stresses, especially at the crystallite boundaries of the ZrO<sub>2</sub> ceramic. These may result in internal cracks and hence, reduction in strength. Therefore, it is important to understand the transition temperature to control the film properties [Moulson and Herbert, 2003].

### 2.3.1 Phase Transformation of Tetragonal $\rightleftharpoons$ Cubic

The  $t \rightarrow c$  phase transition occurs at 2370 °C. The tetragonal phase could be formed by three methods; (1) annealing in the tetragonal stability regime, (2) precipitating from cubic phase, and (3) cubic to tetragonal displacive transformation. The  $c \rightarrow t$  phase transition can be either diffusional or diffusionless in  $ZrO_2$ , depending upon the cooling condition [Yeh et al., 2009]. Figure 2.2 shows that diffusionless  $c \rightarrow t$  phase transition occurs by the oxygen displacement along the  $c$ -axis from the ideal fluorite site [Yashima et al., 1996].

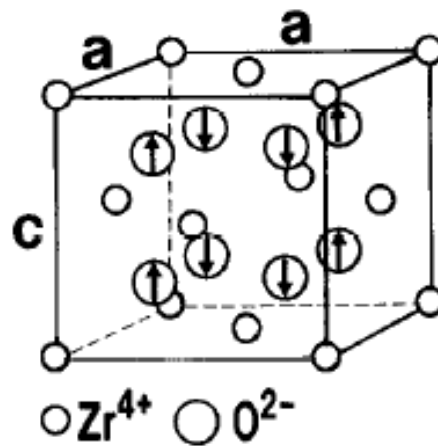


Figure 2.2: A pseudo-fluorite cell of tetragonal zirconia. The arrows show the displacement of the oxygen ions along the  $c$ -axis. [Yashima et al., 1996].

### 2.3.2 Phase Transformation of Monoclinic $\rightleftharpoons$ Tetragonal

The  $t \rightarrow m$  transition occurs between 850 °C and 1000 °C, depending on the surface and strain energies. For the  $m \rightarrow t$  transformation was martensitic in nature. The athermal martensitic transformation from  $m \rightarrow t$  occurs at 1170 °C, associated with shear strain of  $\approx 0.16$  and volume change of 3 – 5 % [Kelly and Francis Rose, 2002; Nazarpour et al., 2010]. Figure 2.3 shows the phase change of  $t \rightarrow m$ .

The transformation of  $t \rightarrow m$  progresses in two stages. The first stage involves a displacive transformation with small shifts of the atoms while the second stage indicated martensitic transformation in which both structures remain almost unchanged. The first transformation stage is destructive and could result in micro cracking resulting in lower mechanical properties [Shackelford and Doremus, 2008].

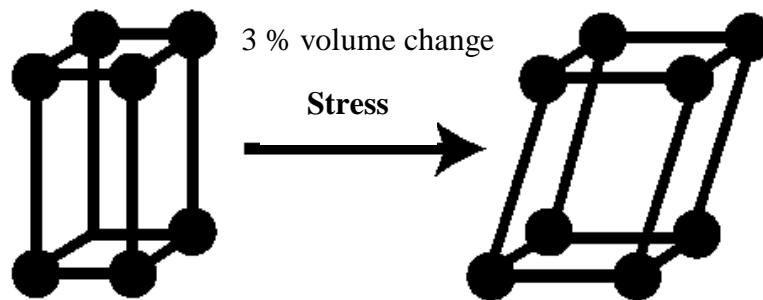


Figure 2.3: Phase change from a tetragonal to monoclinic form [McLaren and Giordano, 2005].

#### 2.4 Stabilizer $ZrO_2$

As discussed earlier, the phase transition ( $t \rightleftharpoons m$ ) induces large volume changes and makes pure  $ZrO_2$  unsuitable for applications involving mechanical strength. Hence, the addition of lower-valence oxides disfavour the formation of monoclinic phase, stabilizing to a more symmetric structures of cubic and tetragonal because of their comparable atomic radii [Patil et al., 2008; Fabris et al., 2002].

The stabilization of  $t-ZrO_2$  can be achieved by: (a) addition of bivalent or trivalent dopants, which induce oxygen vacancies,  $V_o$  (e.g.  $Mg^{2+}$ ,  $Ca^{2+}$ ,  $Gd^{3+}$ ,  $Fe^{3+}$ ,  $Ga^{3+}$  and  $Y^{3+}$ ); (b) tetravalent dopants being undersized or oversized with respect to the oxide cations (e.g.  $Ti^{4+}$ ,  $Ge^{4+}$ ,  $Ce^{4+}$ ); or (c) dopants cause charge-compensations

( $\text{YNbO}_4$ ,  $\text{YTaO}_4$ ). Other minor stabilization mechanism involves matrix constrain of t- $\text{ZrO}_2$  grains held within non-transforming materials [Kellya and Denryb, 2008].

Fully-stabilized zirconia (FSZ) refers to  $\text{ZrO}_2$  that has been completely stabilized in the cubic form. Generally, addition of more than 16 mol% CaO [Muccillo et al., 2001], 16 mol% MgO [Tcheliobou et al., 1996] or 8 mol%  $\text{Y}_2\text{O}_3$  [Kondoh, 2004] would produce FSZ. There would be no phase transformation and it would remain as cubic solid solution from room temperature to about 2500 °C.

The formation of partially stabilized zirconia (PSZ), on the other hand, is dependent on the concentration of stabilizer and the thermal treatment. The common PSZ stabilizer are  $\text{Ca}^{2+}$  (Ca-PSZ) [Tian et al., 2010; Zhou and Ahmad, 2006] and  $\text{Mg}^{2+}$  (Mg-PSZ) [Gocmez and Fujimori, 2008]. In most cases, PSZ is made up of two or more intimately mixed phase, i.e., cubic and tetragonal. Tetragonal zirconia polycrystals (TZP) is  $\text{ZrO}_2$  which has been stabilized in the tetragonal form by the addition of dopants such as  $\text{Ce}^{4+}$  (Ce-TZP) [Mastelaro et al., 2003; Kim et al., 2002] and  $\text{Y}^{3+}$  (Y-TZP) [Viazzi et al., 2006].

#### **2.4.1 Yttria Stabilized Zirconia (YSZ)**

Figure 2.4 show the phase diagram of  $\text{ZrO}_2$ - $\text{Y}_2\text{O}_3$ . It shows the composition fields where the cubic, tetragonal and monoclinic phase is in the stable form and the field where different phases coexist. It gives a better understanding for various properties of the YSZ materials and their behaviour or phase formed when exposed to certain temperatures. Stabilization of the tetragonal and cubic structures requires differing amounts of dopants. The tetragonal phase is stabilized at lower dopant

concentrations while the cubic phase is stabilized at higher dopant concentrations [Shackelford and Doremus, 2008]. Doping of  $Y^{3+}$  has enormous consequences on the properties of  $ZrO_2$  such as hardness (1350  $HV_{30}$ ), bend strength (1000 MPa), compression strength (2000 MPa), Young Modulus (205 GPa) and fracture toughness ( $9.5 \text{ MPa m}^{-1/2}$ ) [Mostaghaci, 1996].

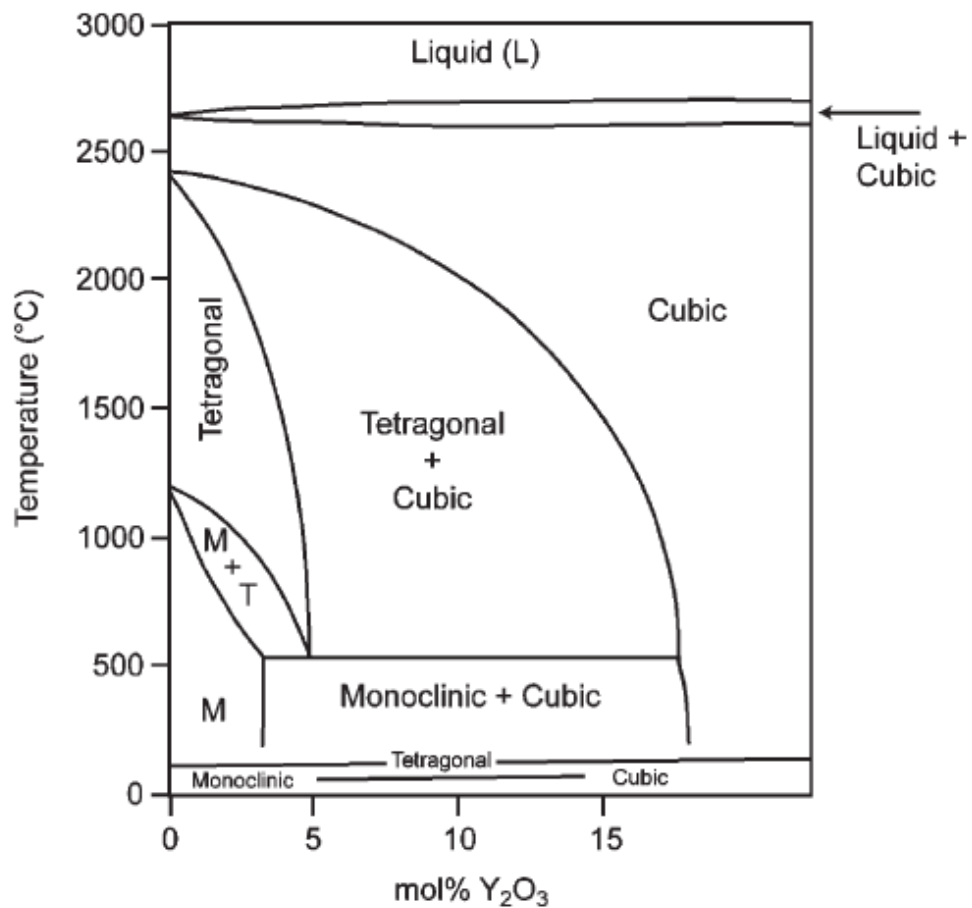


Figure 2.4: Phase diagram for  $ZrO_2$ - $Y_2O_3$  [Shackelford and Doremus, 2008].

When substituting of a trivalent ion,  $Y^{3+}$  ionic radius of 0.1019 nm into  $Zr^{4+}$  ionic radius of 0.084 nm as stabilizer it would result in distorted fluorite structure and an imbalance charge due to larger ionic size of  $Y^{3+}$  and a charge deficiency [Manning et al., 1997]. The addition of trivalent oxide cause some lattice defects like oxygen vacancies  $V_{\text{O}}$  and negatively-charged solutes  $Y'_{\text{Zr}}$ , produced in the  $ZrO_2$  lattice (Figure 2.5). One oxygen vacancy will be created for each pair of dopant cations to maintain charge neutrality [Kelly and Francis Rose, 2002]. The defect structures will then influence the conductivity of stabilized- $ZrO_2$  which results in large increase in ionic conductivity [Vladikova et al., 2006].

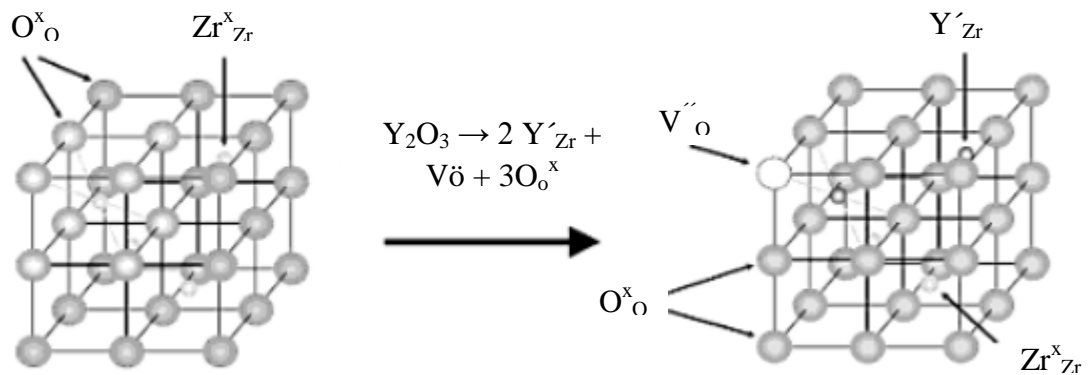


Figure 2.5: Effect of Y doping on  $ZrO_2$  fluorite structure [Peters, 2008].

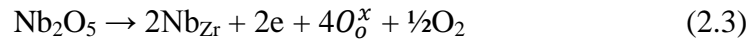
In dilute  $Y_2O_3$  and  $ZrO_2$  solution, the  $(Y'_{Zr} V_{\text{O}})$  is the dominant defect formed as shown in Equation 2.1 [Wang et al., 2000]. The formation of  $(Y'_{Zr} V_{\text{O}} Y'_{Zr})^x$  is possible when high concentration  $Y_2O_3$  added into  $ZrO_2$ . The formations of defect that bind some  $V_{\text{O}}$  to the  $Y'_{Zr}$  sites would cause low conductivity (Equation 2.2) [Vladikova et al., 2006; Lee et al., 1998].





### 2.4.2 Niobia-Yttria Stabilized Zirconia (Nb-YSZ)

Similar to  $Y_2O_3$ ,  $Nb_2O_5$  can only be substitutionally dissolved in  $ZrO_2$ , because it is not interstitially dissolved when considering the relatively large radius of  $Nb^{5+}$  (0.074 nm) with respect to the interstices in the  $ZrO_2$  lattice. The addition of pentavalent oxides would increase the tetragonality (c/a ratio) of  $ZrO_2$  [Guo and Wang, 1997; Lee et al., 1998]. The most probable dissolving mechanism of  $Nb_2O_5$  in  $ZrO_2$  is shown in Equation 2.3.



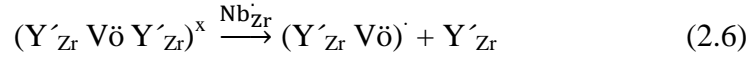
The addition of  $Nb_2O_5$  introduces 2 mol% free electrons for every molar fraction of  $Nb_2O_5$  into YSZ. The following defect reactions (Equation 2.4 and 2.5) show the possible reactions between free electrons and  $V_o$ .



For Equation 2.5, the annihilation of  $V_o$  can be explained by the compensation effect between the acceptor ( $Y_2O_3$ ) and the donor ( $Nb_2O_5$ ).  $Nb^{5+}$  ion on the  $Zr^{4+}$  site implies a net effective of +1 charge, which repels  $V_o$ . The difficulty of the  $V_o$  movement in the YSZ lattices would decrease the mobility of ion and increase the bulk density [Guo and Wang, 1997].

There are other possible defect reactions in the  $Nb_2O_5$  additions. Because of the expected repulsive force between  $Nb_{Zr}^{\cdot}$  and  $V_o$ , then the introduction of  $Nb_{Zr}^{\cdot}$

into YSZ may suppress the formation of the defect associates, even splitting the already formed defect associates, i.e. two defect reactions defined as follows (Equation 2.6 and 2.7) may occur.



The concentration of mobile  $V\ddot{o}$  will increase and the concentration of the only positron-sensitive defect  $(Y'_{Zr} V\ddot{o} Y'_{Zr})^x$  associate in YSZ were decreased [Guo and Wang, 1997].

However, the charge compensation mechanism involved in  $Nb_2O_5$ -YSZ solution is still unknown. There is no clear picture of the microscopic mechanisms of stabilization to parallel the understanding of the mechanism in  $Nb_2O_5$ - $Y_2O_3$ - $ZrO_2$  system: the most relevant issue concerns are the respective roles of impurity cations and oxygen vacancies.

## 2.5 Comparison between Thin Film and Bulk Ceramics

Thin film and bulk ceramics can be prepared by using similar starting sol. Figure 2.6 shows the preparation stages for thin film and bulk ceramics by using a sol-gel method. The formation and deposition methods between thin film and bulk ceramics are the major differences for these two forms. Thin film is the formation of a thin layer of solid material on a solid support, called a substrate by controlled condensation of the individual atomic, molecular, or ionic species, either directly by physical process, or by chemical and/or electrochemical reaction [Soriaga, 2002;

Smith, 1995]. However, the key stages in the production of bulk ceramics are calcinations (powder) and sintering (bulk). The material properties are basically controlled by composition and the grain size or porosity. The calcinated powder would be fabricated to various shape based on the applications. High sintering temperature is required to increase the densification of the bulk material [Moulson and Herbert, 2003].

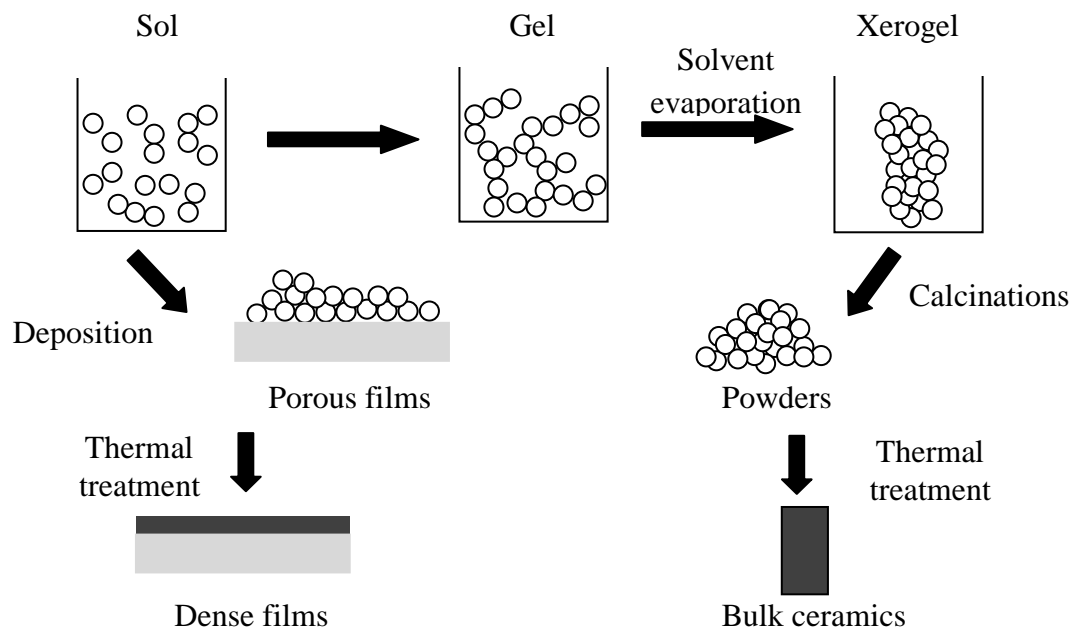


Figure 2.6: Preparation stages for thin film and bulk ceramics by using sol-gel method.

In thin film technology, the difference in properties corresponding to the bulk materials arise because of the small thickness, large surface-to-volume ratio and unique physical structure of the film which are a direct consequence of the growth process. The high surface-to-volume ratio of the thin films and the microstructure can influence a number of phenomena such as gas adsorption, diffusion, and catalytic

activity. In thin film synthesis, the gelling and drying times are much faster than bulk materials because the sample thickness is much smaller. In addition, the coating process may lead to orientation of the polymeric species in the film which is absent in bulk samples. The distances for diffusion are shorter in thin film, and the retention of organic species is expected to reduce [Wasa et al., 2004; Watchman and Haber, 1993].

The presence of a substrate has influence on the thin film development during drying, solvent burnout and densification. Thermal expansion mismatching with the substrate can cause stresses to develop in the thin film. Besides that, the crystallization behaviour of amorphous thin films on the substrate was achieved by surface nucleation and growth of stable or metastable phases at lower temperature than in bulk material. Chemical reactions between the substrate and thin film could also modify the properties and/or performance of the film [Watchman and Haber, 1993].

## **2.6 Thin Film Deposition Technique**

The chemical element or compound would influence the choice of an appropriate thin film deposition. The structure, microstructure, surface and interface morphology, chemical composition and homogeneity are also dependent on the film preparation methods [Beckel et al., 2007]. The deposition techniques of thin film can be discussed in vapour phase deposition and liquid-phase/solution deposition. Pulsed laser depositions (PLD), sputtering and chemical vapour deposition (CVD) are some vapour deposition techniques. On the other hand, the liquid-phase/solution deposition techniques involve chemical solution deposition (CSD) and electrophoretic

deposition (EPD). Table 2.1 shows the deposition techniques and the brief description on the respective techniques.

Table 2.1: Deposition techniques and their respective definition [Beckel et al., 2007].

Deposition technique	Definition
Sputtering	The thin film material is removed from a solid cathode target by bombardment with positively charged ions emitted from a noble gas discharge. The ejected material from target is deposit on substrate.
Pulsed Laser Deposition (PLD)	A pulsed laser beam (wavelength in the UV range) is employed to ablate a target composed of the desired material, which subsequently deposited on substrate.
Chemical Vapour Deposition (CVD)	Evaporation of the precursors that decompose on a hot substrate in a suitable reaction chamber in which the temperature and pressure of gasses was under controlled.
Chemical Solution Deposition (CSD)	The precursor solution was prepared in desired stoichiometric ratio and deposited on the substrate by using spray, spin or dip coating. The as-deposited film is dried, pyrolyzed, crystallized and post-annealed to obtain final product.
Electrophoretic Deposition (EPD)	Powder particles are charged and suspended in a colloidal system. Under the forces of an externally applied electric field, the particles move to the substrate surface and coagulate to form a dense layer.

Thin film coatings of Zr-based ceramic materials are widely used as protective layers against corrosion, wear resistance, thermal barrier coatings or some special electrical functions. YSZ is one of the common Zr-based materials used for these applications. Table 2.2 represents the list of research works using different deposition techniques to fabricate the YSZ films.

Among these techniques, CSD are widely proposed by most authors. CSD are especially attractive because of low cost and mass productivity [Liu et al., 2009]. It

does not required expensive equipment to form a homogeneous film at low temperature [Beckel et al., 2007]. Variety of precursor solution compositions can be produced by deposition on different type of substrates.

Table 2.2: Summary of different deposition techniques used for YSZ films in recent years and the related authors.

Year	Research Group	Deposition technique
2010	Smeacetto et al.	Sputtering
	Tahereh et al.	EPD
	Snieszewski et al.	CSD (Dip-Coating)
2009	Varanasi et al.	CVD
	Liu et al.	CSD (Dip Coating)
2008	Heiroth et al.	PLD
	García-Sánchez et al.	CSD (Spray Deposition)
2007	Briois et al.	Sputtering
	Jiang et al.	CVD
2006	Joo and Choi	PLD
	Jia et al.	EPD
	Chen and Wei	CSD (Spin Coating)
2005	Perednis et al.	CSD (Spray Deposition)
	Samoilenkov et al.	CVD

## 2.7 Chemical Solution Deposition (CSD)

Generally, CSD method involves three important steps: preparation of solution, coating process and annealing. Figure 2.7 shows the processing steps in

CSD method. A variety of parameters must be controlled for each step and these parameters are discussed in the sections below.

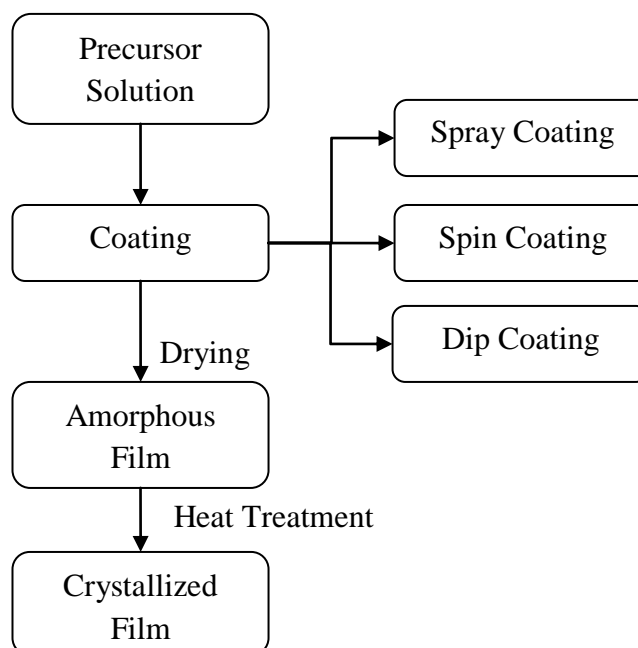


Figure 2.7: Flow Chart of a typical chemical solution deposition (CSD) process.

For the preparation of the solution, the reagent selection (chemical precursor) and solvent choice are important consideration. The chemical precursor dissolved in appreciates solvent to form a homogeneous film and dried at low temperature to form an amorphous film, and heat treated or annealed for densification or microstructure manipulation [Schwartz et al., 2004].

### 2.7.1 Coating Solute

The extremely large choice of precursors is one of the advantages of the CSD technique. In this section, two principal categories of precursor solution, i.e. the metal organic decomposition and sol-gel process were discussed. They are the

common precursor groups used to prepare the Zr-based thin film. The main requirements of coating solution are sufficient solubility of the precursors in the solvent to form a stable coating solution and be able to decompose or maybe pyrolyzed during further thermal processing.

### **2.7.1(a) Metal Organic Decomposition (MOD)**

In this technique, the precursor is a chemical solution containing metal salt and one or more organic species. The organic compounds evaporate partly during or after deposition and the resulting film pyrolyzes upon annealing to form a ceramic coating with desired stoichiometry. Typically, long chain metal carbocylates are used as metal salts and dissolved in an inert solvents, such as xylene. However, the large organic ligands may cause cracking during processing due to the excessive weight loss and shrinkage. The low reactivity of starting reagents also restricts process flexibility. To circumvent this, control of solution concentration and thermal processing is one of the main concerns [Mitzi, 2009; Beckel et al., 2007].

Perednis et al. (2005) investigated the surface morphology of the film prepared by several zirconium salts. He reported that the metal organic salts have higher solubility in organic solvents and gives the better surface quality of film. Neagu et al. (2006) obtained dense, continuous and crack-free YSZ layer by using zirconium acetylacetonate and yttrium chloride.

### **2.7.1(b) Sol Gel Methods**

The sol gel process is based on liquid-phase hydrolysis of organo-metallic salts like metal alkoxides to form a colloidal sol and a condensation step with organic



monomers to form a gel. The particle concentration, viscosity, concentration and stability of sol gel influence the deposition parameters and film quality. The common starting materials used for deposition of sol-gel Zr-based film are alkoxide group and halogenide group.

The authors like Sniezewski et al. (2010), Domínguez-Crespo et al. (2009) and Viazzi et al. (2006) reported used of zirconium alkoxides as starting solution for sol gel deposition techniques. Alkoxides precursors have attracted attention due to their ability to form homogeneous and high quality coatings. However, the shelf-life of sol-gel alkoxides precursors is relatively short and the chemical used are moisture sensitive, thus the precursor synthesis process becomes complicated. So the wet chemistry has to be performed under a protective gas environment. This makes the process costly and difficult to control [Beckel et al., 2007; Aegerter and Mennig, 2004].

For halogenide precursors, the inorganic salts like zirconium oxychloride are used as the starting source in preparing a very stable precursor solution at ambient atmosphere which simplifies the sol gel processing without the protection of inert atmosphere. The halogenide precursor is relatively inexpensive and insensitive to moisture [Aegerter and Mennig, 2004]. From the reported work of Espitia-Cabrera et al. (2008), Arcot and Luo (2008), Baklanova et al. (2007) and Liu et al. (2002), a uniform, crack-free and dense film can be produce by using halogenide precursor.

The sol-gel method was initially developed to prepare submicronic materials with a controlled morphology by using suitable chemical modifications, in which the

conventional solid state chemistry was unable to provide [Carter and Norton, 2007]. Sol-gel route is versatile, relatively simple to transfer at an industrial scale and inexpensive when compared to any deposition technique that involves use of vacuum. The sol gel method is also one of the most important techniques for the formation of various functional coatings. This is due to the excellent control of compositional stoichiometry, the formation of a homogeneous film with a large area and flexible deposition parameters [Chen and Liu, 2002]. The homogeneous film can also be obtained at low temperature. Any excess material in sol gel process can be used again to reduce wasting [Ortiz et al., 2006; Vossan and Kern, 1991].

### **2.7.2 Coating Solvents**

The physical properties of the solution such as boiling point, solubility of salts and spreading behaviour of droplets on the substrate will influence the properties of film. The type of solvents not only influences the salts concentration, but also affects the deposition temperature, optimal solution flow rate and the deposition rate [Perednis et al., 2005]. The solvent should have a moderate viscosity to cover the substrate and keeping the drying time as short as possible. A low surface tension was important to allow a complete wetting of the substrate and form a homogeneous liquid flow. For these reasons, mostly short chained aliphatic alcohols (ethanol, n-propanol, isopropanol, n-butanol) are preferred but others like esters or glycol ethers also can be used in coating technique [Aegerter and Mennig, 2004; Vossan and Kern, 1991].

Ethanol or mixture of ethanol with other solvent was found to be the common solvent used for the preparation of Zr-based thin film. Successful deposition using

different type of solvents like anhydrous ethanol [Liu et al., 2002], ethanol and acetylacetone [Domínguez-Crespo et al., 2009], ethanol and deionized water [Lee et al., 2007], Methyl ethyl ketone–ethanol (MEK-EtOH) [Mauvy et al., 2007] have been reported. Mixtures of different solvents can help to tailor the deposition performance but the phase separation by evaporation has to be avoided which could lead to flow instabilities and wetting problems [Aegerter and Mennig, 2004].

### **2.7.3 Substrate**

The function of substrate is to provide the base and necessary mechanical support for thin film. A cleaned surface of the substrate is important to obtain a high quality film. Different cleaning procedure was needed to guarantee a complete wetting and to avoid surface contamination which inevitably reduces the coating quality. The properties of the substrate such as good surface smoothness and good uniformity are important to grow a defect-free film. The substrate flatness would influence the minimum achievable line width and spacing between the substrate and film. Surface roughness ( $< 10$  nm) [Liu et al., 2002] of the substrate also plays an important role to maintain uniform characteristics of the thin film elements [Elshabini-Riad and Barlow, 1998]. The substrate should have good chemical stability which no deleterious reactions between the film and the substrate.

The different types of substrate used are related to the properties and application of thin film. Huang et al. (2010) reported the YSZ film on Si substrate had potential application as superconductor and capacitor. Amézaga-Madrid et al. (2010) and Xiao et al. (2009) deposited YSZ film on glass substrate for optical application. The others common used substrate materials for YSZ thin films include

stainless steel [Tiwari et al., 2009] and Ni/YSZ substrate [Chen and Wei, 2006] which used as protective coating and solar cells.

#### 2.7.4 Coating Techniques

Once the precursor solution and substrate have been selected, the next step of CSD process is deposit the precursor solution on the substrate. The common coating techniques used to form the thin film are spray coating, spin coating and dip coating as shown in Figure 2.8.

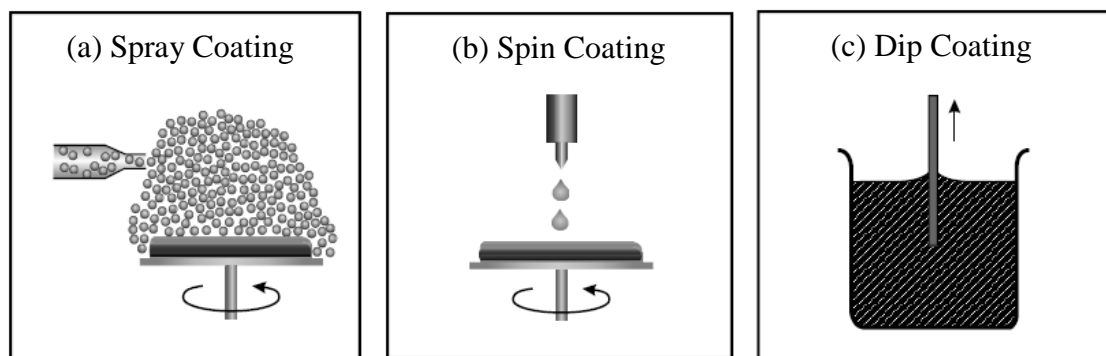


Figure 2.8: The common used coating techniques [Schwartz et al., 2004].

For spray coating (Figure 2.8 (a)), the fine aerosol of a liquid precursor solution is deposit directly toward a heated substrate surface with or without the aid of an external electric field. The deposition efficiency can be obtained by controlled the viscosity and droplet size of precursor solution [Schwartz et al., 2004]. Spin coating consists of applying the solution by rapidly rotating substrate at controlled speed (Figure 2.8 (b)). Spin coating differs from dip coating where the thin films are deposited by centrifugal draining and evaporation. The volatility of the solvent, the initial solution concentration, the spinning rate and speed can control the uniformity and thickness of the film [Stern, 1996; Beckel et al., 2007].